AIAA JOURNAL
Vol. 48, No. 1, January 2010

Laminar Near Wake of a Circular Cylinder at Hypersonic Speeds

Gisu Park,* Sudhir L. Gai,† and Andrew J. Neely‡
University of New South Wales, Australian Defence Force Academy, Canberra, Australian Capital Territory 2600, Australia

DOI: 10.2514/1.44167

The laminar near-wake flow behind a circular cylinder at hypersonic speeds has been examined experimentally and analytically. Surface pressure and heat flux measurements were obtained in a free-piston shock tunnel at a nominal Mach number of 10. The freestream unit Reynolds numbers were 3.02×10^5/m and 11.7×10^5/m at total specific enthalpies of 13.35 and 3.94 MJ/kg, respectively. The experimental data of surface pressure and heat flux showed good agreement with theory based on perfect gas. Unlike surface pressure, the surface heat flux depended strongly on the wall-to-total-temperature ratio, and it increased with increase in the ratio. The surface pressure, however, depended on the Reynolds number, although this dependency was found to be weak. The flow separation angles behind the cylinder showed an inverse of the square root of Reynolds number dependence similar to the low-speed laminar flow separation behind a circular cylinder.

Nomenclature

C	=	Chapman–Rubesin constant, $\rho\mu/\rho_e\mu_e$
c_L	=	centerline
c_p	=	specific heats at constant pressure
c_v	=	specific heats at constant volume
D	=	model diameter
D_{12}	=	diffusion coefficient of a binary gas
E	=	local stagnation enthalpy ratio, $(H/H_e) - 1$
F	=	shear function, Eq. (8)
H	=	local stagnation enthalpy, $h + u^2/2$
H_b	=	total base height of the slender body
H_c	=	total enthalpy in the recirculation region
h	=	static enthalpy
k	=	thermal conductivity
L	=	reattachment distance
Le	=	Lewis number, $\rho D_{12} c_p/k$
M	=	Mach number
Pr	=	Prandtl number, $\mu c_p/k$
p	=	static pressure
Q	=	total surface heat flux
q	=	heat flux, Eq. (1)
R	=	model radius
Re	=	Reynolds number, $\rho u D/\mu$
S	=	reduced streamwise distance, Eq. (10)
S_w	=	parameter S evaluated for body, Eq. (5)
s	=	distance along the free shear layer from flow separation point
T	=	temperature
t	=	time
u	=	velocity
u^*	=	velocity ratio, Eq. (11)
W	=	enthalpy function, Eq. (12)
x	=	distance from the front stagnation point
Y	=	transformed normal distance, Eq. (9)
y	=	distance normal to the wall or dividing streamline
α	=	dissociation fraction
α_R	=	coefficient of resistivity
β	=	Falkner–Skan pressure gradient parameter
γ	=	ratio of specific heats, c_p/c_v
η	=	Howarth and Levy's transformation parameter, Eq. (4)
θ	=	angle from the front stagnation point
μ	=	viscosity
ρ	=	density
$(\rho c_p k)^{1/2}$	=	thermal product
τ	=	nondimensional flow establishment parameter, Eq. (27)
Ω	=	resistance

Subscripts

b	=	base
d	=	dividing streamline
e	=	outer edge of boundary layer
eq	=	equilibrium
est	=	flow establishment
N	=	nitrogen
O	=	oxygen
o	=	total conditions
r	=	reattachment point
sep	=	separation point
stag	=	front stagnation point
w	=	body wall
1	=	conditions ahead of bow shock/freestream
2	=	conditions behind bow shock
3	=	inviscid flow outside free shear layer
4	=	inviscid flow behind wake recompression shock

Received 5 March 2009; revision received 19 August 2009; accepted for publication 21 August 2009. Copyright © 2009 by Gisu Park, Sudhir L. Gai, and Andrew J. Neely. Published by the American Institute of Aeronautics and Astronautics, Inc., with permission. Copies of this paper may be made for personal or internal use, on condition that the copier pay the $10.00 per-copy fee to the Copyright Clearance Center, Inc., 222 Rosewood Drive, Danvers, MA 01923; include the code 0001-1452/10 and $10.00 in correspondence with the CCC.

*Postgraduate Student, School of Aerospace, Civil and Mechanical Engineering.
†Visiting Senior Research Fellow, School of Aerospace, Civil and Mechanical Engineering. Associate Fellow AIAA.
‡Senior Lecturer. School of Aerospace, Civil and Mechanical Engineering. Senior Member AIAA.

I. Introduction

OVER the years, the flow immediately behind blunt bodies, often known as the near wake, has been investigated by various researchers under a broad range of flow regimes varying from subsonic to hypersonic [1–10]. However, a thorough understanding of the near wake at hypersonic speeds, especially at flow conditions that are comparable to reentry-type capsules, still seems limited and remains a challenge.

The near-wake region as defined in this paper extends from the flow separation point to the reattachment point. For blunt bodies such as a circular cylinder, an incoming boundary layer at flow separation forms a free shear layer as the flow detaches from the body surface due to the adverse pressure gradient. The dividing streamline then

separates the flow, which continues to flow downstream of the reattachment point from that, which turns back and recirculates. Figure 1 illustrates a schematic of the near wake behind a circular cylinder.

For blunt bodies that are traveling at high-Mach-number hypersonic speeds, the flow behind a bow shock in the stagnation region becomes subsonic and the temperatures in this region are usually quite high. As a result, the flow is often dominated by chemical reactions such as dissociation and it no longer behaves like a perfect gas [11,12]. As the flow traverses further, the flow accelerates and some recombination may take place. Once the flow separates following an expansion, a free shear layer forms, which is followed by reattachment and recompression during which chemical reaction may or may not dominate. For the near wake behind slender bodies such as wedges and cones, however, the temperature changes are relatively small and dissociation dominated flow is less likely [13–16].

Confining our attention to the near wake behind blunt bodies at hypersonic speeds, there are some experimental [1–10] and theoretical [17,18] studies available. However, the experimental data are usually limited to low-enthalpy cold-tunnel data for which the temperatures are not sufficiently high enough to drive the chemical reactions even on the forebody. In addition, the available theoretical data [17,18] were often validated using these low-enthalpy cold-tunnel data under the assumption of perfect gas. It is therefore of interest to examine the applicability or otherwise of some of the theoretical results and correlations of cold hypersonic data to the present high-enthalpy flow conditions.

Within the framework of laminar near-wake flow, a significant contribution was made by Chapman [19,20]. He introduced the concept of an isentropic recompression of the separated shear layer at the reattachment point. Chapman's method essentially assumes a balance between the mass out flow from the recirculation region to the mass injected into the recirculation region at the reattachment region. This leads to the assumption that the total pressure on the dividing streamline (Fig. 1) must be equal to the static pressure at the reattachment point, so that the part of the shear layer for which the total pressure is less than the static pressure at the reattachment reverts back into the recirculation region and the part of the shear layer for which the total pressure is more than the static pressure at the reattachment point will overcome the recompression shock and flows downstream. The main weakness of the Chapman approach is that it assumes the separating-shear-layer thickness to be zero and the process is fully isentropic. Later, Denison and Baum [21] considered the case with a finite initial boundary-layer thickness (assuming a Blasius initial profile) by solving the momentum equation using a finite difference scheme. However, the validity of these results in high-enthalpy flows, in which the assumption of a perfect gas may not be valid, is not known.

The present paper investigates the near-wake flow behind a circular cylinder at high-enthalpy hypersonic speeds both experimentally and analytically. The theory of Denison and Baum [21] and the extension by Baum et al. [22], which was based on the framework of Chapman [19,20], has been extended to blunt bodies. This includes using more realistic separation profiles at the flow separation point other than using the Blasius profile as an initial profile. Also, the energy balance equation as was used by Baum et al. [22] has been rearranged and applied to the present high-enthalpy experimental conditions.

In the work of Denison and Baum [21] and Baum et al. [22], the assumption of an initial Blasius profile may be justified, because they confined their analyses to slender wedges or rearward-facing steps, in which separation occurs at a sharp corner. In the case of a blunt body such as a cylinder, however, the separation point is not fixed and separation occurs under an adverse pressure gradient. The desirability of using a proper initial profile for the shear layer analysis has been discussed by Dewey [2] and Kubota and Dewey [23], who, however, used an integral approach based on the method of Reeves and Lees [17].

As stated above, herein, the hypersonic laminar near wake behind a cylinder is studied analytically and the results are compared with the experimental data. Alternatively, one could have used a CFD approach and compared the results with experimental data as is the norm at the present time. However, the CFD results, in general, give little insight into the physics of the flow, particularly the effects of varying different flow parameters. Therefore, although not negating the importance of CFD approach, there is still scope for classical analytical methods that enhance our understanding of the problem.

There are several modern asymptotic and other approaches (for example, the momentum integral theory of Reeves and Lees [17] and Kubota and Dewey [23]) that are capable of investigating laminar separated and wake flows. The difficulty, however, with any theory is its validity for various experimental conditions. The asymptotic theory, for example, is strictly valid for very large Reynolds number flows [24]. However, Messiter et al. [25] have shown that the asymptotic approach when applied to even moderate Reynolds number flows can yield surprisingly good agreement with experimental data. Similarly, the momentum integral theory is also shown to yield reasonable results for moderate Reynolds number flows. In the present instance, however, we have applied and extended the approach used by Denison and Baum [21] and Baum et al. [22] (using proper separation profiles) as it is relatively simple and easily modified. The experimental confirmation has justified such an approach, as will be shown in this paper.

This paper deals with three main aspects. First, most of the available existing hypersonic data of the laminar near-wake flow behind a circular cylinder are analyzed in conjunction with the present data. Using the available data, correlations of the near-wake flow features such as base pressure, flow separation angle, and reattachment distance ratio are explicitly investigated. Second, the present experimental data on surface pressure and heat flux are discussed. The experiments were conducted using a free-piston shock tunnel at a nominal Mach number of 10 with freestream unit Reynolds numbers of $3.02 \times 10^5/\text{m}$ and $11.7 \times 10^5/\text{m}$ at total

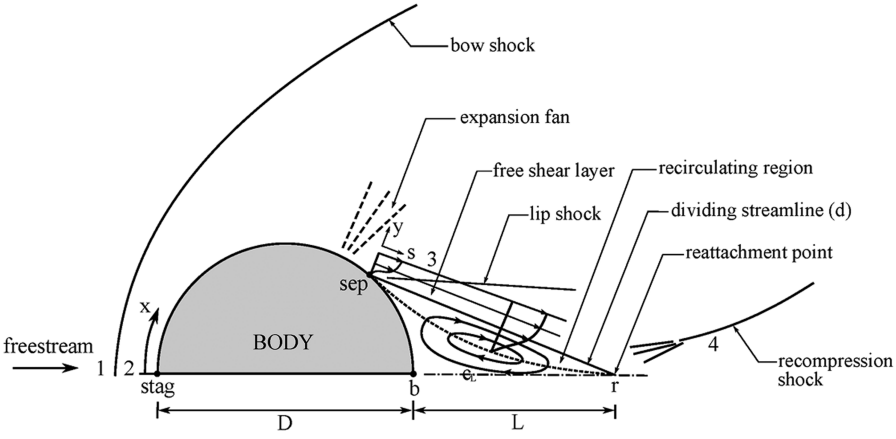

Fig. 1 Schematic of the near wake behind a circular cylinder.

specific enthalpies of 13.35 and 3.94 MJ/kg, respectively. Third, the theory of laminar near-wake flow behind a circular cylinder is discussed. Here, the theory of Denison and Baum [21] and Baum et al. [22] was extended to examine its validity for high-enthalpy flows under an assumption of perfect gas. A comparison between the theory and the present experimental data as well as the existing hypersonic data is then presented.

II. Experimental Details

A. Flow Facility

The experiments were conducted using a free-piston shock tunnel T-ADFA located in the School of Aerospace, Civil, and Mechanical Engineering, University of New South Wales at the Australian Defence Force Academy in Canberra. Figure 2 shows a schematic of the T-ADFA free-piston shock tunnel.

It was operated under a reflected mode in which the free-piston compresses the driver gas almost isentropically. Following the first diaphragm burst, the shock wave travels through the shock tube. The shock speeds were monitored using pressure transducers that were mounted in the wall of the shock tube. The nozzle reservoir pressure was monitored by a transducer that was mounted just upstream of the nozzle inlet. Upon reflection of the shock wave from the shock tube end, the test gas expanded through the nozzle and reached the model. The duration of steady periods ranged from approximately 150–400 μs, after which the measurements became unreliable due to flow contamination [26].

B. Models and Instrumentation

The circular cylinder had an outer diameter of 32 mm and the span was 132 mm. It was supported by side struts with chamfered end plates on both sides to minimize end effects. The sensors were located every 20° apart along the azimuth and the measurements were taken every 10° by rotating the model. A sketch of the model is shown in Fig. 3. It will be noted that the aspect ratio of the model is only 4.1. This was necessary because it was thought desirable to contain the exposed surface of the model to be within the nozzle inviscid core, which was about 180 mm in diameter, and the nozzle exit diameter was 305 mm. The implications of the finite aspect ratio are discussed in Sec. IV.

The surface heat fluxes around the forebody were measured using K-type surface junction thermocouples. The K-type thermocouples were chosen for the forebody heat flux study, as they are quite robust and have relatively fast signal responses. They consisted of a chromel wire fitted coaxially within a hollow cylinder of Alumel. The outer diameter of each thermocouple was 2 mm and its length was 10 mm. Sandpaper was used to form a junction, resulting in tiny strands between the end of dissimilar metals. The resistance of the junctions was approximately 1.4 Ω, and the sensitivity of the sensor was found to be 40 μV/K at room temperature [27].

In the base region, however, the surface heat fluxes were measured using thin-film gauges. They consisted of thin films of platinum, which were applied to the surface of a Macor substrate that had negligible thermal conductivity. The diameter of the Macor was 2 mm and its length was 4 mm. Detailed descriptions of manufacturing the gauges can be found in [28]. The thin-film gauges were chosen to measure the surface heat flux in the base region due to the nature of the flow and due to the fact that thin films have a much higher signal-to-noise ratio than thermocouples.

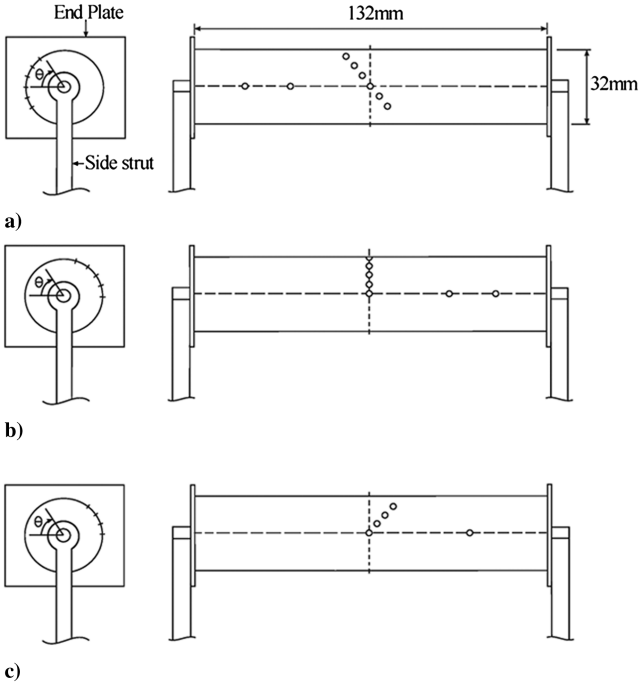

Fig. 3 Circular cylinder models: a) thermocouples, b) thin-film gauges, and c) pressure transducers.

The surface heat flux is based on the measured time history of temperature, which can be calculated using the relation [27]

$$q(t_n) = \frac{2(\rho c_p k)^{1/2}}{\pi^{1/2}} \sum_{i=1}^{n} \frac{T(t_i) - T(t_{i-1})}{(t_n - t_i)^{1/2} + (t_n - t_{i-1})^{1/2}} \qquad (1)$$

where $T(t_i) = V(t_i)/\alpha_R$, and $(\rho c_p k)^{1/2}$ is known as the thermal product of the substrate. The thermocouples were calibrated using a water-dipping technique [29], and $(\rho c_p k)^{1/2}$ was determined to be 9690 ± 300 Ws$^{0.5}$/m^{2}K. For thin-film gauges, $(\rho c_p k)^{1/2}$ was determined to be 1500 ± 120 Ws$^{0.5}$/m^{2}K through the dynamic calibration using a shock tunnel. The coefficient of resistivity α_R was found to be 1.52 ± 0.08 mV/K through the static calibration using a furnace. The typical resistances of the gauges were 120–150 Ω. Detailed descriptions regarding the gauge calibration can be found in [28,30].

The surface pressures in the near wake were measured using XCS-093 series Kulite pressure transducers. These were capable of measuring the pressures in the range of 0 to 34.5 kPa. Each transducer had a diameter of 2.4 mm and its length was 9.5 mm. The sensitivity of the sensors was 3.66 ± 0.044 mV/kPa. The sensors were flush-mounted. The front stagnation pressures were measured using a 113M165 series PCB Piezotronics pressure transducer. It had a sensitivity of 7.48 mV/kPa. The transducer was cavity mounted with a diameter of 1.4 mm and a depth of about 1 mm.

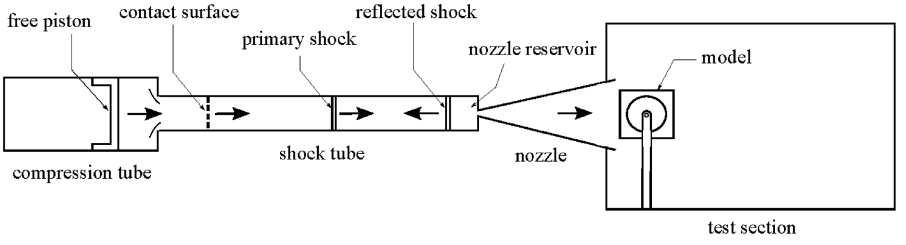

Fig. 2 Schematic of the T-ADFA free-piston shock tunnel.

Table 1 Flow conditions

	Condition A	±%	Condition B	±%
Nozzle reservoir properties				
p_o, MPa	11.1	7.0	11.3	4.3
T_o, K	6918	2.8	3154	1.4
Freestream properties				
u_1, m/s	4556	2.2	2588	1.0
M_1	9.13	2.9	10.30	1.8
ρ_1, g/m^3	2.0	17.5	6.0	10.9
p_1, Pa	381	21.4	291	14.7
T_1, K	593	8.8	168	5.3
H_o, MJ/kg	13.35	4.4	3.94	1.8
Re_1, 1/m	3.02×10^5	13.4	11.7×10^5	8.8
α_O	0.71	——	0.01	——
α_N	0	——	0	——
Postshock properties				
α_O	1	——	0.13	——
α_N	0.076	——	0	——

C. Flow Conditions

The experiments were conducted using two flow conditions. The models were located 10 mm downstream from the nozzle exit. The test gas was air throughout. In view of the high Mach numbers and moderate Reynolds numbers, the flows were considered laminar. Also, the characteristic unsteadiness usually associated with transitional and turbulent flows was not observed from either the surface pressure or heat flux signal traces.

Table 1 summarizes the nozzle reservoir and freestream properties that were used for the present study. The uncertainties (±%) in the table denote the standard deviations of the properties based on the 95% confidence interval. In the calculation of freestream Reynolds number, the viscosity μ_1 was obtained using curve-fit data [31] based on the Lennard-Jones potential.

The nozzle reservoir properties were calculated using the computer program ESTC [32], which assumes chemical and vibrational equilibrium throughout. ESTC calculates the nozzle reservoir conditions at the end of the shock tube by matching the reflected shock pressure to the measured reservoir pressure under an assumption of thermodynamic equilibrium.

The freestream properties were calculated using the quasi-one-dimensional nozzle flow code STUBE [33]. The calculations were made by assuming chemical nonequilibrium, and the excitation of vibrational modes were assumed to be frozen at specified temperatures. The inputs to the code were the nozzle reservoir pressure, reservoir temperature, and the nozzle geometry. For this study, a conical nozzle was used that had a 7.5° half-angle, 12.7 mm throat, and 305 mm exit diameter. To account for the growth of the boundary layers along the nozzle, STUBE was run until the calculated and measured pitot pressures matched. The equivalent divergence angles of the nozzle were $6.9 \pm 0.3°$ for both flow conditions.

The postshock properties were calculated using EQSTATE [34]. The inputs to the code were the freestream pressure, velocity, temperature, and flow deflection angle. In the calculation, it was assumed that the flow deflection angles were 0° following the normal shock assumption, and the flows were considered as equilibrium upstream of the bow shock wave. With condition A, the flow behind the shock wave was highly dissociated with all oxygen dissociated ($\alpha_O = 1$) and some nitrogen dissociated ($\alpha_N = 0.076$). With condition B, there was a small amount of oxygen dissociation ($\alpha_O = 0.13$) and no nitrogen dissociation.

III. Theory of Laminar Near Wake

A. Velocity and Enthalpy Profiles at Flow Separation Point

Cohen and Reshotko [35] proposed that the equations for a two-dimensional steady compressible laminar boundary layer of a perfect gas can be simplified to a set of nonlinear ordinary differential equations through Stewartson's transformation with a power-law velocity distribution. After the boundary-layer equations are simplified, the equations for momentum and energy can be expressed as follows.

Momentum equation:

$$f''' + ff'' = \beta(f'^2 - 1 - E) \tag{2}$$

Energy equation:

$$E'' + PrfE' = (1 - Pr)\left[\frac{(\gamma - 1)M_{e,\text{sep}}^2}{1 + \frac{(\gamma-1)}{2}M_{e,\text{sep}}^2}\right][f'f''' + f''^2] \tag{3}$$

where $E = (H/H_e) - 1$, β is the Falkner-Skan pressure gradient parameter, $M_{e,\text{sep}}$ is the Mach number at the edge of the boundary layer at the flow separation point, and $f' = u/u_e$. The primes denote differentiation with respect to η, where η is the normal distance parameter defined in terms of Howarth and Levy's transformation as [11,21,22],

$$\eta = \frac{\rho_e u_e}{(2S_w)^{1/2}} \int_0^y \frac{\rho}{\rho_e} \mathrm{d}y \tag{4}$$

where

$$S_w = \int_0^{x_{\text{sep}}} C\rho_e u_e \mu_e \mathrm{d}x \tag{5}$$

S_w is the reduced streamwise distance evaluated for the body, and $C = \rho\mu/\rho_e\mu_e$ is the Chapman–Rubesin constant.

In solving Eqs. (2) and (3) for the present case, the Prandtl number was taken to be 0.72, and γ was taken to be 1.4 assuming perfect gas. $M_{e,\text{sep}}$ was calculated using an inviscid isentropic flow relation and it was determined to be 3.36 and 3.42 for the flow conditions A and B, respectively.

It is well known that in incompressible flow, $\beta = 0$ for a flat-plate flow and $\beta = 1$ in the immediate vicinity of a stagnation region of two-dimensional bodies [35]. When $\beta < 0$, the flows are affected by adverse pressure gradients. For a compressible flow with an isothermal wall, Reeves and Lees [17] have shown that the Falkner–Skan equation can be solved under the assumption $-0.5 \le \beta \le 0$. For a compressible flow of perfect gas with a Prandtl number of unity, Cohen and Reshotko [35] have shown that the flow separates at $\beta = -0.326$ with a cold wall, where $E_w = -0.8$. For the present flow conditions A and B, the corresponding values of β were calculated as -0.36 and -0.35, respectively. The corresponding E_w values were -0.96 and -0.9, respectively.

Equations (2) and (3) were solved using a multiple-shooting method [36] using the fourth-order Runge–Kutta scheme [35]. The equations were iterated by assuming an initial value for β and $E'(0)$. After iterating the equations using several sets of initial values, an interpolation was carried out to estimate the next guess of the initial values. The process was repeated until the following boundary conditions were satisfied:

At $\eta \to 0$,

$$f(0) = f'(0) = f''(0) = 0, \qquad E = E_w$$

At $\eta \to \infty$,

$$f'(\infty) = 1, \qquad E(\infty) = 0$$

where $E_w = (H_w/H_e) - 1$. The equations were solved for the interval $0 \le \eta \le 7$ with 1000 node points across η. The iterations were terminated when $(f'(\infty) - 1) \le 1e^{-5}$ and $E(\infty) \le 1e^{-5}$. The convergence of solutions was checked by doubling the size of η, and it was found that the differences were negligible.

Figure 4 presents the velocity and enthalpy profiles at the separation point for the present flow conditions. The Blasius velocity profile and the Crocco integral profiles used by Denison and Baum [21] and Baum et al. [22] are also shown for comparison. It should be noted that the enthalpy profiles based on the Crocco integral (as used by Baum et al. [22]) and as shown in Fig. 4b are wall-temperature-dependent.

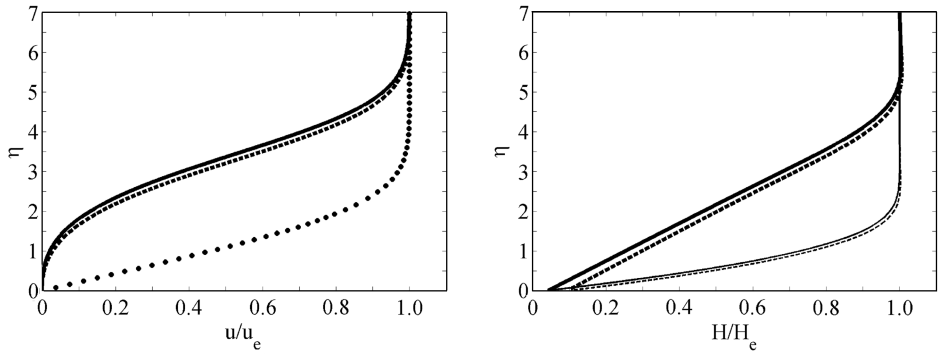

Fig. 4 Flow separation profiles: a) velocity ratio and b) enthalpy ratio; condition A, $T_w/T_o = 0.04$ (thick solid line); condition B, $T_w/T_o = 0.1$ (thick dashed line); Blasius profile (dotted line); Crocco integral profile, condition A (solid line); and Crocco integral profile, condition B (dashed line).

A feature to note in Figs. 4a and 4b is that the differences in velocity as well as enthalpy distributions between the flow conditions seem to be quite small. However, the differences between the profiles of the present data to the Blasius and the Crocco integral profiles are quite significant. The influences of these differences on base pressure and heat flux are discussed in Sec. IV.

B. Analysis of Free Shear Layer

After applying the Howarth and Levy transformations [21], the boundary-layer equations that govern the flow in the free shear layer become, after Denison and Baum [21] and Baum et al. [22],

Momentum equation:

$$u^* \frac{\partial F}{\partial CS} = F^2 \frac{\partial^2 F}{\partial u^{*2}} \tag{6}$$

Energy equation:

$$u^* \frac{\partial H}{\partial CS} = F^2 \frac{\partial^2 H}{\partial u^{*2}} \tag{7}$$

where

$$F = \frac{\partial u^*}{\partial Y} \tag{8}$$

$$Y = \rho_e u_e \int_0^y \frac{\rho}{\rho_e} \mathrm{d}y \tag{9}$$

$$S = \int_0^s C \rho_e u_e \mu_e \mathrm{d}s \tag{10}$$

$$u^* = \frac{u}{u_e} \tag{11}$$

Assumptions:

$$Pr = Le = 1 \quad \text{and} \quad C = \rho\mu/\rho_e\mu_e = \text{const}$$

$F(S, u^*)$ is a shear function, $H(S, u^*)$ is the total enthalpy, Y is the transformed normal distance, S is the reduced streamwise distance measured from the flow separation point, and C is the Chapman–Rubesin constant.

Denison and Baum [21] assume that the pressure gradients in the shear layer are negligible in order to uncouple the momentum and energy equations. Assuming that the same assumption is valid in the present case, we can solve the uncoupled momentum and energy equations.

Equations (6) and (7) were solved using a second-order implicit finite difference method [21]. As noted by Denison and Baum [21], the stability of the calculation can be improved using S centered finite difference approximations for derivatives with respect to u^*. In solving Eq. (7), H was replaced by a nondimensional enthalpy function W, where

$$H_e - H = (H_e - H_w)W + (H_e - H_c)(W_0 - W) \tag{12}$$

Here, H_c is the total enthalpy in the recirculation region and $W_0 = [(H_e - H)/(H_e - H_w)]_{s=0}$ is the initial enthalpy function at the separation point. Unlike Baum et al. [22] who used the Crocco integral profile as an initial profile, the present study used the separation profile as an initial profile that was calculated using Eqs. (2) and (3) from the preceding section.

The shear layer calculations were programmed using commercial software MATLAB, and 1000 mesh points were used for u^*. The convergence of solutions was checked by doubling the size of u^* and it was found that the differences were negligible.

Once the shear layers were computed, the dividing streamline velocity ratio u_d^* was calculated. The initial values for u_d^* and F_d at the separation point were

$$u_d^* \frac{\mathrm{d}u_d^*}{\mathrm{d}S} = F_d \left(\frac{\partial F}{\partial u^*} \right)_d = 0 \tag{13}$$

Figure 5 presents the profiles of transformed shear and enthalpy functions of the free shear layer for condition B. The general characteristics of the shear layer profiles were the same for condition A.

In regard to Fig. 5, it can be seen that the distributions of the shear as well as the enthalpy functions become flatter as S increases. At $S/S_w \to \infty$, the distributions of the shear function reach the Chapman profile. Also, the dividing streamlines for both the shear and the enthalpy functions tend to reach the Chapman limit ($u^* = 0.587$) at $S/S_w \to \infty$. It is interesting to note the differences in the dividing streamline shape compared to that computed by Denison and Baum [21], wherein at the start of the shear layer the shear function has a finite value as a consequence of the Blasius profile assumption.

Figure 6 shows the variation of the velocity ratio u_d^* along the dividing streamline. In the figure, the comparison is made between the present shear layer profiles and the Blasius profile. Chapman's limiting value of $u^* = 0.587$ is also indicated on the figure. Initially, the Blasius profile shows higher values of u_d^* due to its finite shear at separation. Beyond $S/S_w \approx 10^{-2}$, however, the present data shows higher values of u_d^*. The difference between the two present profiles and the Blasius profile becomes quite small beyond $S/S_w \approx 10^0$, all asymptotically tending toward the Chapman limit.

C. Base Pressure

Assuming that Chapman's isentropic recompression [20] at the reattachment point and constant pressure mixing assumption [19] hold in the recirculation region, the base pressure is found as

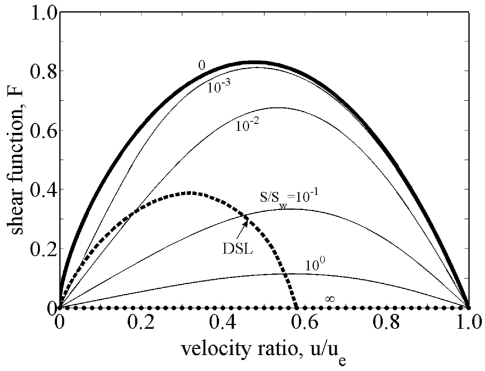

a)

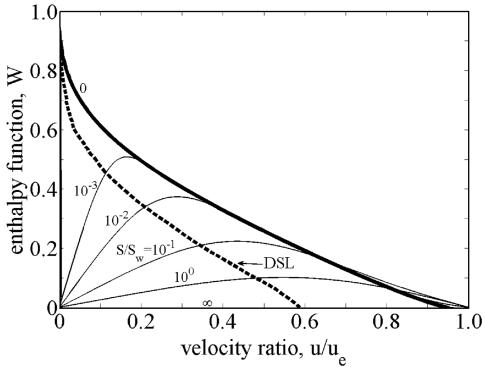

b)

Fig. 5 Shear and enthalpy function profiles for flow condition B: a) shear function and b) enthalpy function; separation profile (thick solid line), dividing streamline (DSL) (thick dashed line), and Chapman profile (dotted line).

$$\frac{p_t}{p_e} = \frac{p_4}{p_b} = \left[1 + \frac{(\gamma - 1)}{2} M_d^2\right]^{\gamma/\gamma - 1} \tag{14}$$

where

$$M_d = u_d / \sqrt{\gamma R T_d} \tag{15}$$

As noted by Dewey [2], the assumption of isentropic recompression becomes strictly unrealistic if the extent of the separation and recompression regions become comparable to the thickness of the free shear layer, for example, at very low Reynolds numbers (Re_{3D}) and very high Mach numbers ($M_{3,e}$). Crocco and Lees [37] have shown that the recompression is a function of Reynolds number, but in many cases, this dependence is found to be weak. For the present data, the Reynolds numbers Re_{3D} were 4×10^3 and 1×10^4, and the Mach numbers $M_{3,e}$ were 2.82 and 2.92 for

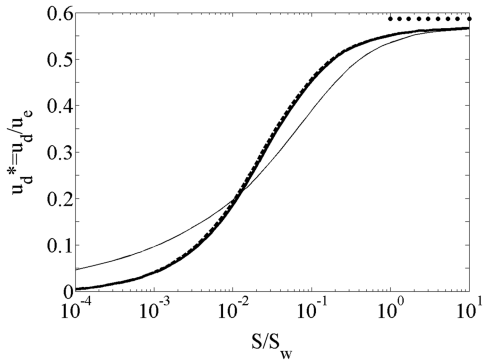

Fig. 6 Variation of u_d^* along the dividing streamline; condition A, $T_w/T_o = 0.04$ (thick solid line); condition B, $T_w/T_o = 0.1$ (thick dashed line); Blasius profile (solid line); and Chapman limit [19], $u^* = 0.587$ (dotted line).

conditions A and B, respectively. Here, $M_{3,e}$ was calculated using the experimental data [26] under the assumption of isentropic inviscid flow from the separation point to the reattachment point.

According to Kubota and Dewey [23], the dividing streamline temperature ratio for isoenergetic flow can be expressed as

$$\frac{T_d}{T_e} = 1 + \frac{(\gamma - 1)}{2} M_e^2 (u_d^* - u_d^{*2}) \tag{16}$$

where T_d is the temperature in the recirculation region and T_e is the external shear layer static temperature.

The Mach number M_d is calculated from Eqs. (15) and (16), where u_d^* was obtained from the free-shear-layer calculations.

The pressure behind the wake recompression shock can be obtained using an isentropic inviscid flow relation:

$$\frac{p_{t4}}{p_4} = \left[1 + \frac{(\gamma - 1)}{2} M_4^2\right]^{\gamma/\gamma - 1} \tag{17}$$

Using Chapman's relation [20],

$$M_4^2 = (1 - u_d^{*2}) M_e^2 \tag{18}$$

The base pressure ratio may be expressed as

$$\frac{p_b}{p_{\text{stag}}} = \frac{p_b}{p_{t2}} = \frac{p_b}{p_4} \times \frac{p_4}{p_{t4}} \times \frac{p_{t4}}{p_{t3}} \times \frac{p_{t3}}{p_{t2}} \tag{19}$$

For this study, it is assumed that an isentropic inviscid flow assumption holds along the streamline at the outer edge of the boundary layer from the front stagnation point of the body through the shear layer so that $p_{t3}/p_{t2} = 1$. The total pressure loss (p_{t4}/p_{t3}) across the recompression shock was obtained using an oblique shock relation (the wake shock angles required for this were obtained from the schlieren data in [26]).

Combining Eqs. (14) and (17–19), we obtain

$$\frac{p_b}{p_{\text{stag}}} = \frac{p_{t4}}{p_{t3}} \left[\left(1 + \frac{(\gamma - 1)}{2} M_d^2\right) \left(1 + \frac{(\gamma - 1)}{2} (1 - u_d^*) M_e^2\right) \right]^{\gamma - 1/\gamma} \tag{20}$$

D. Base Heat Flux

To derive an expression for the base heat flux, an understanding of the energy balance in the near wake is required. As noted by Baum et al. [22], the energy balance in the near wake is expressed as

$$\underbrace{\left[-\int_0^\infty (H_e - H) \rho u \, dy \right]_{\text{sep}}}_{E_{\text{in}}} = \underbrace{\left[-\int_{y_d}^\infty (H_e - H) \rho u \, dy \right]_r}_{E_{\text{out}}} + q_b \tag{21}$$

Here, E_{in} is the energy from the boundary layer that enters into the free shear layer at the flow separation point, E_{out} is the energy above the dividing streamline that leaves downstream of the reattachment point, and q_b is the energy into the shear layer, recirculation zone, and to the base wall. Figure 7 illustrates the energy balance in the near wake behind a circular cylinder.

Rearranging Eq. (4) and substituting it into the first integral E_{in} from Eq. (21) yields

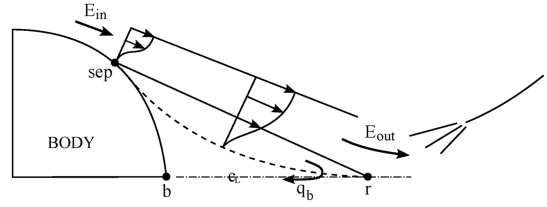

Fig. 7 Sketch of the energy balance in the near wake behind a circular cylinder.

$$E_{\text{in}} = \left[-(2S_w)^{1/2} \int_0^{\infty} (H_e - H) u^* \mathrm{d}\eta \right]_{\text{sep}} \tag{22}$$

In order to calculate E_{in} from Eq. (22), the value of u^* as determined in the previous section was used.

The second integral E_{out} can be simplified by transforming the y coordinate to the u^* coordinate. Rearranging Eq. (9) and substituting it into Eq. (8) yields

$$\int_0^{\infty} \rho \mathrm{d}y = \frac{1}{u_e} \int_0^1 \frac{1}{F} \mathrm{d}u^* \tag{23}$$

Since E_{out} is the energy integral from the dividing streamline to the outer edge of the free shear layer at the reattachment point, Eq. (23) can be expressed as

$$\int_{y_d}^{\infty} \rho \mathrm{d}y = \frac{1}{u_e} \int_{u_d^*}^1 \frac{1}{F} \mathrm{d}u^* \tag{24}$$

Substituting Eq. (24) into the second integral E_{out} of the energy balance yields

$$E_{\text{out}} = \left[-\int_{u_d^*}^1 (H_e - H) \frac{u^*}{F} \mathrm{d}u^* \right]_r \tag{25}$$

Therefore, the base heat flux can be expressed as

$$q_b = \left[-(2S_w)^{1/2} \int_0^{\infty} (H_e - H) u^* \mathrm{d}\eta \right]_{\text{sep}} + \left[\int_{u_d^*}^1 (H_e - H) \frac{u^*}{F} \mathrm{d}u^* \right]_r \tag{26}$$

The base heat flux calculated from using the above expression is next compared to the experimental data.

IV. Results and Discussion

A. Flow Establishment

Figure 8 shows typical traces of surface pressure and heat flux of a circular cylinder at the front stagnation point, separation point, and center of the base for condition B. The general characteristics of the flow were the same for condition A as well. The steep gradients of the signals in the beginning of the flow for both pressures and heat fluxes are due to the shock arrival. The flow then requires a sufficient time to establish and become steady. After the establishment of the steady period, an expansion fan arrives and terminates the flow. The shot-to-shot variations of the signals in the near wake at various azimuthal positions during the steady flow were approximately ±6 and ±9% for pressure and heat flux, respectively.

The time to establish the steady flow is usually characterized using a nondimensional parameter [38,39]:

$$\tau_{\text{est}} = \frac{t_{\text{est}} u_1}{D} \tag{27}$$

where τ_{est} denotes the number of body lengths of flow required to establish steady flow. Here, t_{est} is the time required to reach steady flow, u_1 is the freestream velocity, and D is the model diameter. For the present study, the flows were considered to be steady when the mean values reached 95 and 90% of their final values for pressure and heat flux, respectively.

Figure 9 presents the distributions of the flow establishment time for pressure and heat flux behind the circular cylinder. From the figure, it is seen that it requires about 50 to 66 body lengths to establish steady pressures behind the cylinder. On the other hand, the heat flux data indicate a gradual increase in body length required for the establishment of steady flow from the separation point downstream before reaching a plateau toward the rear stagnation point at $\theta = 180°$. It is seen that, on average, it requires about 90 body lengths to reach steady-state heat flux in the base region.

We may note that while flow establishment times for pressure measurements are nearly the same for all angular positions, those for heat flux differ considerably, the differences being of the order of 20 to 30% as the flow progresses from $\theta = 90$ to 180°.

B. Surface Pressure Measurements

Some surface pressure data around the forebody at hypersonic speeds are shown in Fig. 10. These are compared with the existing numerical [40,41] and experimental [6] data. The numerical data were based on an inviscid calculation in which the equations of motion were solved using an ordinary differential equation under the assumption of perfect gas with an adiabatic wall. In regard to the present data, the measured surface pressures are quite sparse. This was due to the fact that some of the Kulite sensors, which are quite fragile, were damaged under the harsh environment such as flying debris from the ruptured diaphragm.

It is seen that the present forebody pressure data show reasonable agreement with these numerical and experimental data. It is also noted that both Mach number and wall temperature effects are weak in this region.

The surface pressure distributions on the base of the cylinder are shown in Fig. 11. Here, the experimental data are compared with the results of present theory as well as the theory of Chapman [19] and Denison and Baum [21]. The theoretical calculations of Grange et al. [18], based on the integral method of Reeves and Lees [17], are also included for comparison. The Grange et al. [18] calculation assumes a perfect gas and adiabatic wall.

Concerning the experimental data, it is seen that there is a distinct local minimum at 130 and 120° from the front stagnation point for

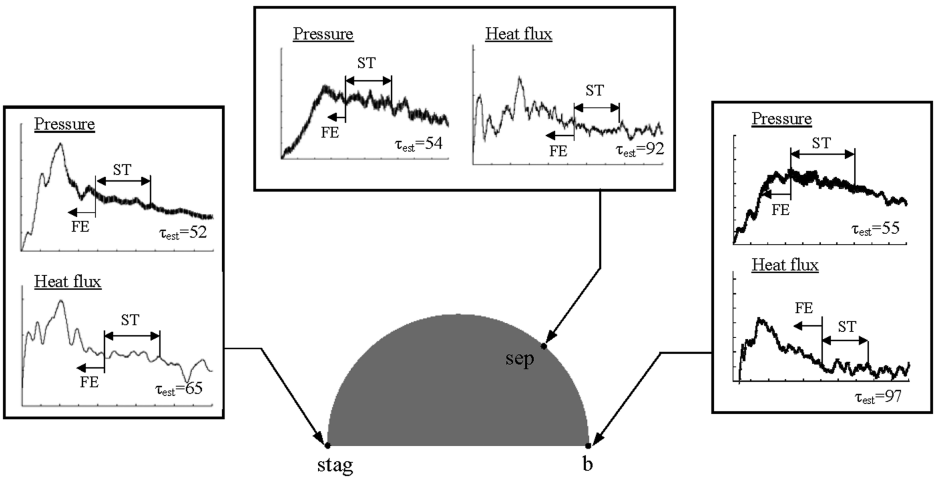

Fig. 8 Typical traces of surface pressure and heat flux around a circular cylinder; ST denotes steady flow and FE denotes flow establishment.

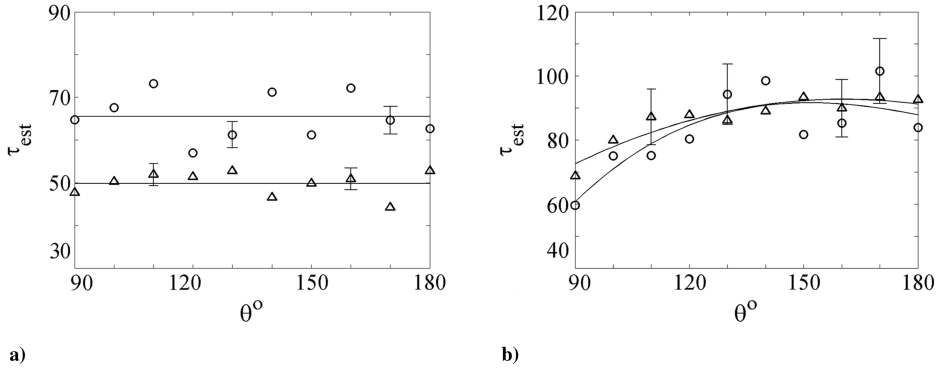

Fig. 9 Flow establishment time for pressure and heat flux behind a circular cylinder: a) pressure and b) heat flux; condition A (○) and condition B (△), curve fit through experimental points (solid line).

conditions A and B, respectively. The distributions then show gradual recovery up to approximately 150°, after which they attain a plateau. This pressure distribution is consistent with the observation of Dewey [2]. Again, as with the forebody pressures, effects of Mach number and wall temperature seem to be weak.

Further, it is seen that the results of the present theory show a very good agreement with the experimental data, as does the Grange et al. [18] theory. It is interesting to note that there is a gradual improvement of base pressure prediction from Chapman (zero boundary thickness) to Denison and Baum [21] (Blasius initial profile) and to the present theory (separation profile). This would indicate the importance of using a proper separation profile in the computation of the base pressure. The good agreement between experimental data and theory also shows that as far as pressures are concerned, real gas effects are small.

Figure 12 shows the base pressure variation with Reynolds number Re_{2D}, where Re_{2D} is based on cylinder diameter and postshock conditions [42], so that

$$Re_{2D} = Re_{1D}\left(\frac{\mu_1}{\mu_2}\right) \tag{28}$$

This figure contains the existing cylinder data and covers a broad range of Mach and Reynolds numbers. Table 2 summarizes the experimental conditions for these data.

From Fig. 12, we note that while there is some dependency of the base pressure on Reynolds number at supersonic speeds (based on the data of Walter and Lange [7]), the base pressure dependency at hypersonic speeds is quite small in the Reynolds number range covered ($10^3 \leq Re_{2D} \leq 10^4$). This is consistent with the Mach number independence principle at hypersonic speeds, as also noted earlier by Dewey [2] and Tewfik and Giedt [5]. The present data shown are seen to be somewhat lower than others. The possible reason for this is discussed in the following paragraphs.

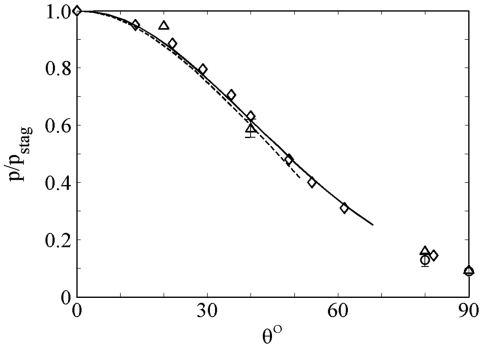

Fig. 10 Surface pressure distributions around the forebody; present data: condition A, $T_w/T_o = 0.04$ (○), and condition B, $T_w/T_o = 0.1$ (△); Token and Oguro [6], $T_w/T_o = 1$ (◇); Fuller [40], inviscid calculation, $M_1 = \infty$, $\gamma = 1.4$, and $T_w/T_o = 1$ (dashed line); Belotserkovskii [41], inviscid calculation, $M_1 = 5$, $\gamma = 1.4$, and $T_w/T_o = 1$ (solid line).

In Sec. II, mention was made of the small aspect ratio of the model and its possible effects on the measured data. Figure 13 shows the effect of aspect ratio on the base pressure. The present data are shown in comparison with the California Institute of Technology (Caltech) cylinder data, in which aspect ratio is explicitly stated. Dewey [2] suggested that the base pressure is fairly independent of the cylinder diameter (and hence Re_{2D}) if the model aspect ratio is not less than about 10. The somewhat lower base pressures measured in the present experiments are therefore likely to be the consequence of the small aspect ratio of the model of these experiments.

Although the differences are not very large in absolute terms, they are significant when expressed in percentage terms. The fact that the experimental surface pressures on the base of the cylinder show such good agreement with theory (Fig. 11) is therefore surprising. This discrepancy is still unresolved.

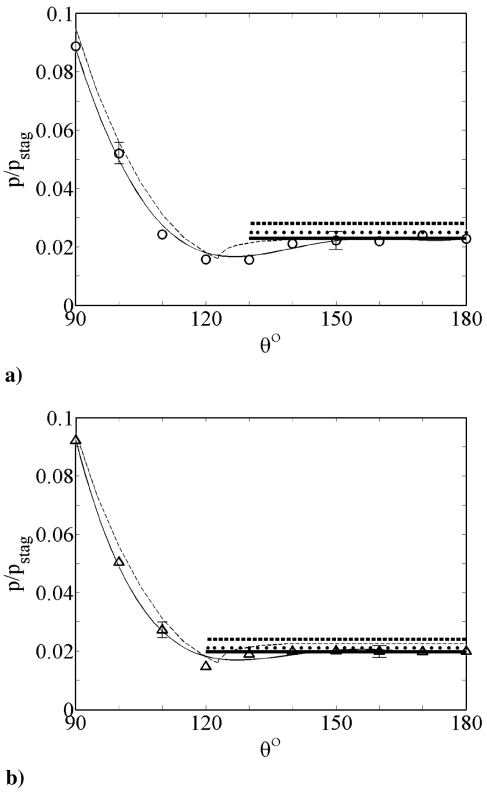

Fig. 11 Surface pressure distributions on the base of the cylinder: a) condition A and b) condition B; present data: condition A, $T_w/T_o = 0.04$ (○), and condition B, $T_w/T_o = 0.1$ (△); Grange et al. [18] (integral theory, $T_w/T_o = 1$) (dashed line); present theory (thick solid line); Denison and Baum [21] (theory, Blasius profile) (dotted line); Chapman [19] (theory, $u^* = 0.587$) (thick dashed line); and curve fit through experimental points (solid line).

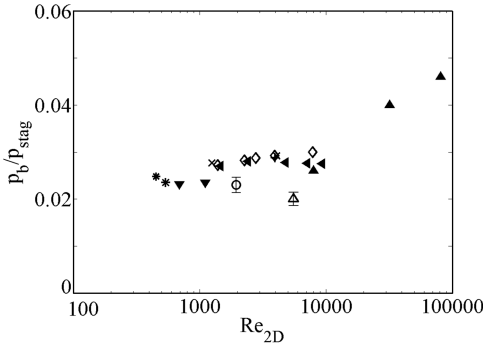

Fig. 12 Variation of circular-cylinder base pressures with Reynolds number at supersonic and hypersonic speeds; present data for condition A (○) and condition B (△), Tewfik and Giedt [5] (*), Dewey [2] (◇), McCarthy and Kubota [4] (◀), Token and Oguro [6] (▼), Herzog [3] (+), Collins et al. [1] (×), and Walter and Lange [7] (▲).

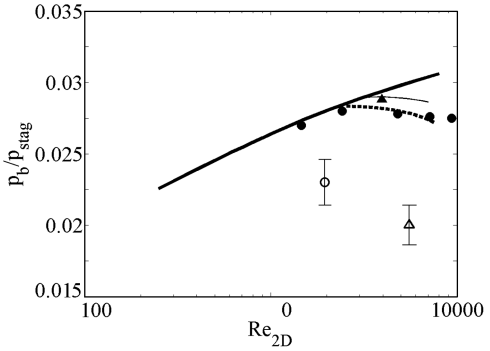

Fig. 13 Influence of aspect ratio on base pressure; present data, AR = 4.1, for condition A (○) and condition B (△), Herzog [3], AR = 40 (▲); McCarthy and Kubota [4], AR = 15 (●); Dewey [2], experimental, AR ≥ 20 (thick solid line); Dewey [2], experimental, AR = 10 (thick dashed line); and Collins et al. [1], experimental, AR = 15 (solid line); AR denotes the aspect ratio.

C. Surface Heat Flux Measurements

Figure 14 presents the surface heat flux distributions around the forebody of a circular cylinder ($0° \le \theta \le 90°$). The error bars denote the shot-to-shot variations of the averaged steady heat flux. The present data are compared with the theory of Lees [11] and the hypersonic experimental data of Koppenwallner [43] and Tewfik and Giedt [5]. The theory of Lees [11] was based on thermal equilibrium under an assumption of a cold wall, for which the surface heat flux was driven purely by thermal conduction.

The surface heat flux distributions seem to show a dependence on wall temperature. The heat flux seems to increase with the increase in wall-to-stagnation-temperature ratio. This trend is not so strong in the front stagnation region ($\theta \le 30°$) but is more prominent beyond $\theta > 30°$.

Lees [11] gave the heat flux around the cylinder as

$$q_{\text{eq}} \cong 0.5 Pr^{-2/3} (\rho_e \mu_e)_o^{0.5} u_1^{0.5} H_o F(S) \tag{29}$$

where

$$F(S) = \frac{(1/2^{0.5})(p/p_{\text{stag}})(\mu T_o/\mu_o T)(u_e/u_1)}{[\int_0^x (p/p_{\text{stag}})(u_e/u_1)(\mu T_o/\mu_o T)\mathrm{d}x]^{0.5}} \tag{30}$$

For the front stagnation point, the expression of Fay and Riddell [12] has been used:

$$q_{\text{stag,eq}} = 0.57 Pr^{-0.6} (\rho_w \mu_w)^{0.1} (\rho_e \mu_e)^{0.4} (H_e - H_w)(\mathrm{d}u_e/\mathrm{d}x)_{\text{stag}}^{0.5} \tag{31}$$

In the calculation of surface heat flux at the front stagnation point, the velocity gradient KD/u_1 of 1.14 was used, where $K = (\mathrm{d}u_e/\mathrm{d}x)_{\text{stag}}$. This seems a reasonable assumption, as the gradient plateaus at hypersonic speeds [44,45]. In solving Eq. (30), the present experimental data were used for p/p_{stag} and the isentropic flow relations were used to calculate the thermodynamic properties around the body. The surface heat fluxes at the front stagnation point measured in the present experiments were 6.68 and 1.51 MW/m^2 for conditions A and B, respectively. The theoretical heat flux obtained using Eq. (31) was found to be 6.69 MW/m^2 and 1.55 MW/m^2. Considering the shot-to-shot variations of the present data, which was approximately 9%, it is quite reasonable to conclude that the surface heat flux at the front stagnation point of the present data are in thermal equilibrium.

Figure 15 presents the surface heat flux distributions in the base of the cylinder. The data from Tewfik and Giedt [5] are also shown for comparison.

Again, the wall temperature effect similar to that on the forebody is seen. Similar to the pressure data described earlier, the heat flux distributions also show a trend toward local minima, indicating flow separation (at approximately 140 and 130° for conditions A and B, respectively), but it is not as distinct as in the pressure distributions. This is then followed by a slight recovery (up to about $\theta \approx 160°$) and a plateau thereafter. The Tewfik and Giedt data [5], shown here, do not indicate any dip or plateau. Again, it is noted that agreement with theory is good, although the theory is based on perfect gas assumption. As with the pressure data, there is a slight improvement of the base heat flux prediction by the present theory compared with that of Baum et al. [22].

Figure 16 shows the dependence of base heat flux on freestream Reynolds number. The present data are compared with the theoretical slender-body data of Baum et al. [22]. The cylinder data of Tewfik and Giedt [5] are also included for comparison. In the figure, Q_b denotes the total surface heat flux from the flow separation point to the base, Q_w is the total surface heat flux from the front stagnation point to the separation point, and D denotes the diameter of the cylinder as well as the total base height of the slender body.

First, the blunt-body base heat flux is significantly higher than that of slender bodies at similar Reynolds numbers. Second, both blunt- and slender-body base heat flux is strongly dependent on wall-to-stagnation-temperature ratio, increasing with the increase in this ratio. There seems to be no systematic variation with the freestream Mach number.

D. Flow Separation Angles

Figure 17 presents flow separation angles behind a circular cylinder at hypersonic speeds from various sources, including the present data. For this representation, the separation angles were

Table 2 Circular cylinders: existing data on base pressures

Investigator	M_1	Re_{2D}	T_w/T_o	ASPECT RATIO	Facility
Collins et al. [1]	6	$(1.25–4.08) \times 10^3$	0.93	15	Wind tunnel
Dewey [2]	6	$(0.36–7.89) \times 10^3$	0.95	10–36	Wind tunnel
Herzog [3]	6.08	3.95×10^3	0.9	40	Wind tunnel
McCarthy and Kubota [4]	5.7	$(0.68–10.16) \times 10^3$	0.95	15–45	Wind tunnel
Tewfik and Giedt [5]	4.19–5.73	$(4.53–5.4) \times 10^2$	0.3–0.95	N/A	Wind tunnel
Token and Oguro [6]	14	$(0.69–1.11) \times 10^3$	∼1	N/A	Wind tunnel
Walter and Lange [7]	2.48–4.92	$(0.8–8.1) \times 10^4$	0.92	N/A	Wind tunnel
Present data	9.13–10.3	$(2.06–5.18) \times 10^3$	0.04–0.1	4.1	Shock tunnel

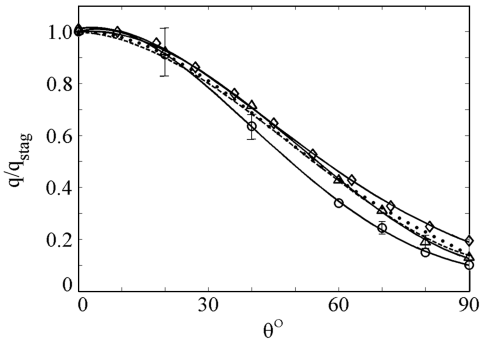

Fig. 14 Surface heat flux distributions around the forebody; present data: condition A, $T_w/T_o = 0.04$ (○), and condition B, $T_w/T_o = 0.1$ (△); Tewfik and Giedt [5], $T_w/T_o = 0.3$ (◇); Lees [11], theory, thermal equilibrium (dotted line); Koppenwallner [43], $T_w/T_o = 0.2$ (dashed line); and curve fit through experimental points (solid line).

assumed to be at the pressure minima of the distributions [2,4,5]. Thus, the separation angles were estimated from the measured pressure distributions presented in the papers by the various authors quoted. There is therefore some uncertainty in these estimates. However, it is believed that they are not seriously in error. The numerical results of Bashkin et al. [46] based on the Navier–Stokes equations assuming perfect gas are also included for comparison.

Figure 17a presents the separation angles in terms of Re_{2D}, as defined earlier. In Fig. 17b, they are plotted in terms of Reynolds number Re_{wD}, as suggested by Potter [47], to show the influence of wall temperature. Re_{wD} is defined as

$$Re_{wD} = Re_{2D}\left(\frac{\mu_2}{\mu_w}\right) \tag{32}$$

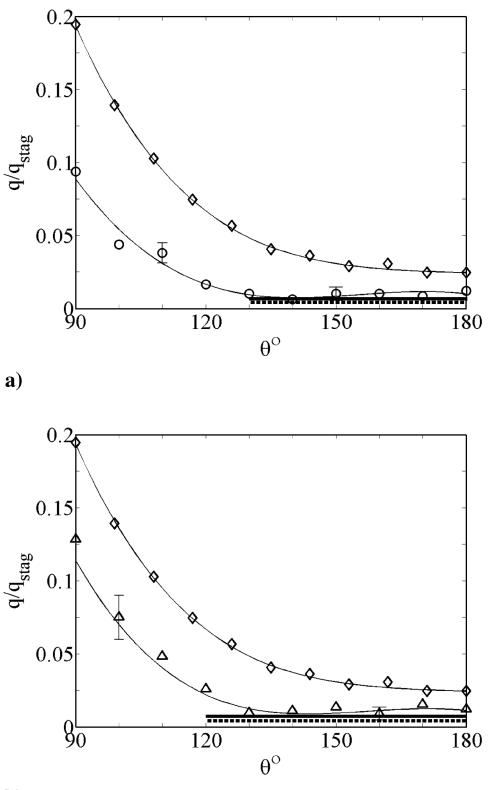

Fig. 15 Surface heat flux distributions in the base region: a) condition A; b) condition B; present data: condition A, $T_w/T_o = 0.04$ (○), and condition B, $T_w/T_o = 0.1$ (△); Tewfik and Giedt [5], $T_w/T_o = 0.3$ (◇); present theory (thick solid line); Baum et al. [22], theory (thick dashed line); and curve fit through experimental points (solid line).

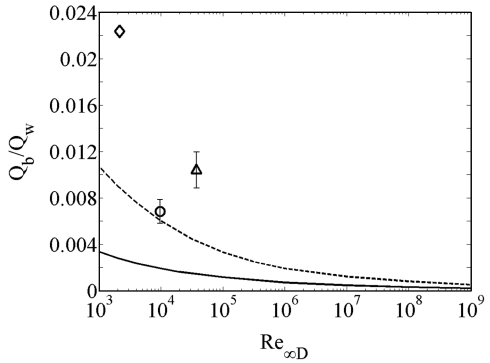

Fig. 16 Dependence of base heat flux on Reynolds number; condition A, $M_\infty = 9.13$, $T_w/T_o = 0.04$ (solid line); condition B, $M_\infty = 10.3$, $T_w/T_o = 0.1$ (△); Tewfik and Giedt [5], cylinder, $M_\infty = 5.5$, $T_w/T_o = 0.3$ (◇); Baum et al. [22], theory, wedge, $M_\infty = 20$, $T_w/T_o = 0.02$ (thick solid line); Baum et al. [22], theory, wedge, $M_\infty = 4$, $T_w/T_o = 0.25$ (thick dashed line).

First, considering Fig. 17a, there appears to be a linear relationship between the separation angle and the inverse of the square root of Reynolds number. However, closer inspection reveals that while there is a good correlation with the adiabatic-wall data, the cold-wall data of the present, Tewfik and Giedt [5], and that of Bashkin et al. [46] show some scatter.

To assess the influence of wall temperature, the data are shown plotted in Fig. 17b in terms of the Reynolds number Re_{wD} defined as above. We note that while all the adiabatic-wall data again correlate

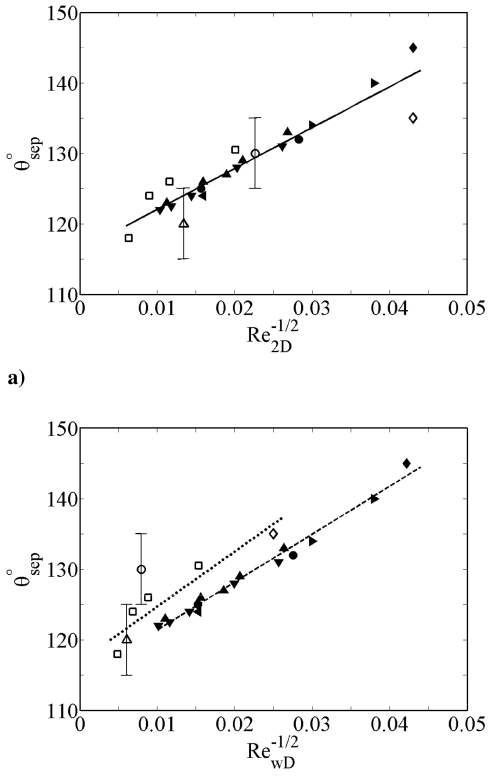

Fig. 17 Laminar flow separation angles behind a circular cylinder at hypersonic speeds for $\theta_{sep} = 577.0 + 116.3Re_{2D}^{-1/2}$ (thick solid line); cold wall: present data, condition A, $T_w/T_o = 0.04$ (○); present data: condition B, $T_w/T_o = 0.1$ (△); Tewfik and Giedt [5], $T_w/T_o = 0.3$ (◇); Bashkin et al. [46], $T_w/T_o = 0.5$, numerical results (□); $\theta_{sep} = 780.4 + 116.9Re_{wD}^{-1/2}$ (dotted line); adiabatic wall: Tewfik and Giedt [5] (◆); Dewey [2] (▲); McCarthy and Kubota [4] (▼); Token and Oguro [6] (▶); Herzog [3] (◀); Collins et al. [1] (●); and $\theta_{sep} = 679.0 + 114.6Re_{wD}^{-1/2}$ (thick dashed line).

well, the cold-wall data are now well separated from the adiabatic-wall data. They too seem to show a near-linear relationship, except for the data of high-enthalpy condition A. The reason for this discrepancy is not known at present. Based on the data presented in Figs. 17a and 17b, the relationship between the laminar separation angle and the cylinder Reynolds number, either Re_{2D} or Re_{wD}, can be described as follows:

$$\theta_{\text{sep}} = 577.0 + 116.3Re_{2D}^{-1/2} \tag{33a}$$

or for adiabatic-wall data,

$$\theta_{\text{sep}} = 679.0 + 114.6Re_{wD}^{-1/2} \tag{33b}$$

and for cold-wall data,

$$\theta_{\text{sep}} = 780.4 + 116.9Re_{wD}^{-1/2} \tag{33c}$$

when

$$5.4 \times 10^2 \leq Re_{2D} \leq 2.5 \times 10^4$$

or

$$5.6 \times 10^2 \leq Re_{wD} \leq 4.3 \times 10^4$$

It is interesting to note that such a linear relationship between the flow separation angle and the cylinder Reynolds number is also found in low-speed laminar flow around a cylinder [48]:

$$\theta_{\text{sep}} = 101.5 + 155.2Re_D^{-1/2} \tag{34}$$

Wu et al. [48] established this relationship based on their experiments in the Reynolds number range of $10 \leq Re_D \leq 2 \times 10^2$.

E. Reattachment Distance

Another important characteristic of the near wake of blunt bodies is the reattachment distance, which is considered next. Figure 18 shows the reattachment distance as a function of the freestream Reynolds number $Re_{\infty D}$ at hypersonic speeds. It presents results of blunt bodies such as circular cylinders and blunt bases of slender bodies such as cones and wedges. Only laminar flow data are considered. The theoretical results of adiabatic and cold walls by Reeves and Lees [17] for a circular cylinder are also included. In the figure, L denotes the distance of the reattachment point from the base, D denotes the diameter of the cylinder, and H_b denotes the total base height of the slender body. Again, in this figure, as in Fig. 17, some of the data were explicitly given by the authors and some were estimated. Hence, some uncertainties may be present.

As seen from the figure, the reattachment distance behind a cylinder seems dependent on the freestream Reynolds number and the wall temperature based on the Reeves and Lees [17] theory. The dependency seems weaker with the cold wall. The mostly near-adiabatic-wall data from the Caltech group seem to be generally consistent with the adiabatic-wall theory. However, in view of the uncertainty in the estimation of the reattachment distance, the agreement can be considered fair at best.

The present cold-wall data taken from [26], in which the experiments were conducted using the same facility and model, and the flow conditions with $T_w/T_o = 0.04$ (condition A) and $T_w/T_o = 0.1$ (condition B) fall roughly in the region of Reeves and Lees [17] cold-wall theory although the theory is calculated for a specific value of $T_w/T_o = 0.2$. It is conceivable, however, that were the calculations to be made based on the theory for $T_w/T_o = 0.04$ and 0.1, the corresponding theoretical curves would pass through the experimental points. That they happen to be close to the slender-body data is fortuitous. All one can say, therefore, is that the present data are generally consistent with the existing cylinder data, which, in any case, is still sparse.

In contrast to the cylinder, the reattachment distance for blunt bases of slender bodies, such as cones and wedges, seems independent of both Reynolds number and wall temperature, a feature that does not seem to have been pointed out previously.

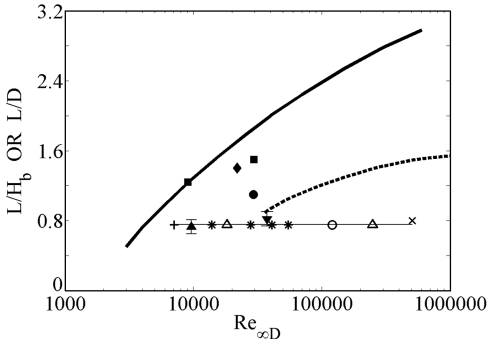

Fig. 18 Variation of reattachment distance ratios with Reynolds number at hypersonic speeds; circular cylinders: Dewey [2], $T_w/T_o = 0.95$ (◆); Collins et al. [1], $T_w/T_o = 0.93$ (■); Herzog [3], $T_w/T_o = 0.9$ (●); Park et al. [26], $T_w/T_o = 0.04$ (▲); Park et al. [26], $T_w/T_o = 0.1$ (▼); slender bodies: Todisco and Pallone [13], $T_w/T_o = 0.125$ (+); Batt and Kubota [49], $T_w/T_o = 1$ (*); Zakkay and Cresci [50], $T_w/T_o = 0.32$ (×); Muntz and Softley [15], $T_w/T_o = 0.18$–0.25 (△); Murman [16], $T_w/T_o = 1$ (○); Reeves and Lees [17], theory, adiabatic wall (thick solid line); Reeves and Lees [17], theory, $T_w/T_o = 0.2$ (thick dashed line); and curve fit through experimental points for slender bodies (solid line).

V. Conclusions

The flow over a circular cylinder in moderate- to high-enthalpy hypersonic flow has been investigated with particular emphasis on the laminar near wake. The results may be summarized as follows:

The forebody data of surface pressure and surface heat flux showed good agreement with the previous hypersonic data and theory based on perfect gas in the case of pressures and thermal equilibrium in the case of surface heat flux. Unlike pressures, the heat flux data showed a strong effect of wall-to-stagnation-temperature ratio.

Concerning the near wake, the pressure data were consistent with the previous hypersonic cold-tunnel data. In particular, the pressure distribution showed a minimum (indicative of separation) and then a gradual recovery before reaching a plateau. The pressure distribution in the separated region showed very good agreement with the theories based on Denison and Baum [21] and Baum et al. [22], but assuming an initial separation profile based on the Cohen and Reshotko [35] approach. While the original theory of Denison and Baum [21] and Baum et al. [22] was developed for blunt-based slender bodies such as cones and wedges, it has been shown here to be equally applicable to a blunt-body wake. The present theory and experimental data also showed fair agreement with the integral theory of Grange et al. [18].

The heat flux data also showed a distribution similar to the pressure in that the flow separation was indicated by a minimum followed by a small recovery and a plateau. There was good agreement with the theory.

The angle at which the flow separates from the cylinder at hypersonic speeds showed a linear relationship with the inverse of the square root of the Reynolds number. A similar relationship is known to exist in low-speed flow over a circular cylinder. Its validity in cylinder flows at hypersonic speeds is shown for the first time.

The reattachment distance behind the cylinder showed a dependency on the Reynolds number as well as the wall temperature. This is unlike that observed for the blunt bases of slender bodies, wherein the reattachment distance seems to be independent of both the Reynolds number and the wall-to-stagnation-temperature ratio.

To conclude, the present study has shown that in moderate- to high-enthalpy hypersonic flows, wherein chemical reactions may be dominant on the forebody, their effects on the base region seem to be not very significant. For such chemical reactions to be dominant in the base region, much higher-enthalpy and Mach number environments are needed. Facilities that produce such environments and of

sufficient duration to make reliable measurements are, at present, very sparse.

Acknowledgments

This work forms part of the project Physics of Base Flows of Planetary Configurations, which is supported by the Australian Research Council, to whom grateful thanks are expressed. The authors are grateful to F. Foppoli and P. Walsh for constructing the models and running the shock tunnel. The authors are also grateful to R. Hruschka and N. R. Deepak for helpful discussions.

References

[1] Collins, D. J., Lees, L., and Roshko, A., "Near Wake of a Hypersonic Blunt Body with Mass Addition," *AIAA Journal*, Vol. 8, No. 5, 1970, pp. 833–842. doi:10.2514/3.5775

[2] Dewey, C. F., "Near-Wake of a Blunt Body at Hypersonic Speeds," *AIAA Journal*, Vol. 3, No. 6, 1965, pp. 1001–1010. doi:10.2514/3.3045

[3] Herzog, R. T., "Nitrogen Injection into the Base Region of a Hypersonic Wake," Eng. Thesis, California Inst. of Technology, Pasadena, CA, 1964.

[4] McCarthy, J. F., and Kubota, T., "A Study of Wakes Behind a Circular Cylinder at $M_\infty = 5.7$," *AIAA Journal*, Vol. 2, No. 4, 1964, pp. 629–636. doi:10.2514/3.2399

[5] Tewfik, O. K., and Giedt, W. H., "Heat Transfer, Recovery Factor, and Pressure Distributions Around a Circular Cylinder Normal to a Supersonic Rarefied-Air Stream," *Journal of the Aerospace Sciences*, Vol. 27, No. 10, 1960, pp. 721–729.

[6] Token, K. H., and Oguro, H., "Experimental Investigations of Hypersonic Flow Around Two-Dimensional Circular Cylinders," Univ. of Cincinnati, Aerospace Research Labs., Rept. 65-212, Cincinnati, OH, Oct. 1965.

[7] Walter, L. W., and Lange, A. H., "Surface Temperature and Pressure Distributions on a Circular Cylinder in Supersonic Cross-Flow," Naval Ordnance Lab., Rept. 2854, White Oak, MD, June 1963.

[8] Koppenwallner, G., and Wuest, W., "The Hypersonic Low Density Wind-Tunnel of the Aerodynamische Versuchsanstalt Gottingen—Operational Behavior and Results on Vibrational Relaxation," 6th Aerospace Sciences Meeting, AIAA Paper 1968-49, New York, Jan. 1968.

[9] Hollis, B. R., "Experimental and Computational Aerothermodynamics of Mars Entry Vehicle," Ph.D. Thesis, North Carolina State Univ., Raleigh, NC, 1996; also NASA CR 201633, 1996.

[10] Holden, M. S., Chadwick, K. M., Gallis, M. A., and Harvey, J. K., "Comparison Between Shock Tunnel Measurements on a Planetary Probe Configurations and DSMC Predictions," *Proceedings of the 20th International Symposium on Shock Waves*, California Inst. of Technology, Pasadena, CA, July 1995, pp. 179–184.

[11] Lees, L., "Laminar Heat Transfer over Blunt-Nosed Bodies at Hypersonic Flight Speeds," *Jet Propulsion*, Vol. 26, No. 4, 1956, pp. 259–269.

[12] Fay, J. A., and Riddell, F. R., "Theory of Stagnation Point Heat Transfer in Dissociated Air," *Journal of the Aerospace Sciences*, Vol. 25, No. 2, 1958, pp. 73–85.

[13] Todisco, A., and Pallone, A. J., "Near Wake Flow Field Measurements," *AIAA Journal*, Vol. 3, No. 11, 1965, pp. 2075–2080. doi:10.2514/3.3317

[14] Todisco, A., Pallone, A., and Heron, K., "Hot-Wire Measurements of the Stagnation Temperature Field in the Wake of Slender Bodies," Research and Advanced Development Div., Avco Corp., Rept. RAD-TM-64-32, Wilmington, MA, July 1964.

[15] Muntz, E. P., and Softley, E. J., "A Study of Laminar Near Wakes," *AIAA Journal*, Vol. 4, No. 6, 1966, pp. 961–968. doi:10.2514/3.3588

[16] Murman, E. M., "Experimental Studies of a Laminar Hypersonic Cone Wake," *AIAA Journal*, Vol. 7, No. 9, 1969, pp. 1724–1730. doi:10.2514/3.5382

[17] Reeves, B. L., and Lees, L., "Theory of Laminar Near Wake of Blunt Bodies in Hypersonic Flow," *AIAA Journal*, Vol. 3, No. 11, 1965, pp. 2061–2074. doi:10.2514/3.3316

[18] Grange, J., Klineberg, J. M., and Lees, L., "Laminar Boundary-Layer Separation and Near-Wake Flow for a Smooth Blunt Body at Supersonic and Hypersonic Speeds," *AIAA Journal*, Vol. 5, No. 6, 1967, pp. 1089–1096. doi:10.2514/3.4142

[19] Chapman, D. R., "Laminar Mixing of a Compressible Fluid," NACA TN-1800, 1950.

[20] Chapman, D. R., Kuehn, D. M., and Larson, H. K., "Investigation of Separated Flows in Supersonic and Subsonic Streams with Emphasis on the Effect of Transition," NACA TR 1356, 1958.

[21] Denison, M. R., and Baum, E., "Compressible Free Shear Layer with Finite Initial Thickness," *AIAA Journal*, Vol. 1, No. 2, 1963, pp. 342–349. doi:10.2514/3.1535

[22] Baum, E., King, H. H., and Denison, M. R., "Recent Studies of the Laminar Base-Flow Region," *AIAA Journal*, Vol. 2, No. 9, 1964, pp. 1527–1534. doi:10.2514/3.55084

[23] Kubota, T., and Dewey, C. F., "Momentum Integral Methods for the Laminar Free Shear Layer," *AIAA Journal*, Vol. 2, No. 4, 1964, pp. 625–629. doi:10.2514/3.2398

[24] Neiland, V. Ya., Bogolepov, V. V., Dudin, G. N., and Lipatov, I. I., *Asymptotic Theory of Supersonic Viscous Gas Flows*, Elsevier Aerospace Engineering Series, Butterworth-Heinemann, London, 2008.

[25] Messiter, A. F., Hough, G. R., and Feo, A., "Base Pressure in Laminar Supersonic Flow," *Journal of Fluid Mechanics*, Vol. 60, No. 3, 1973, pp. 605–624. doi:10.1017/S0022112073000376

[26] Park, G., Hruschka, R., Gai, S. L., and Neely, A. J., "Flow Establishment Behind Blunt Bodies at Hypersonic Speeds in a Shock Tunnel," *Proceedings of SPIE: The International Society for Optical Engineering*, Vol. 7126, 2008, Paper 71260I. doi:10.1117/12.822751

[27] Schultz, D. L., and Jones, T. V., "Heat Transfer Measurements in Short-Duration Hypersonic Facilities," AGARD No 165, Neully-sur-Seine, France, 1973.

[28] Kinnear, K., and Lu, F. K., "Design, Calibration and Testing of Transient Thin Film Heat Transfer Gauges," 20th AIAA Advanced Measurement and Ground Testing Technology Conference, AIAA Paper 98-2504, Albuquerque, NM, June 1998.

[29] Mallinson, S. G., "Shock Wave/Boundary Layer Interaction at a Compression Corner in Hyper-Velocity Flows," Ph.D. Thesis, Univ. of New South Wales, Canberra, Australia, 1994.

[30] Hayne, M. J., "Hypervelocity Flow Over Rearward-Facing Steps," Ph.D. Thesis, Univ. of Queensland, Brisbane, Australia, 2004.

[31] Neely, A. J., "Planetary Entry Aerothermodynamic Studies in a Superorbital Expansion Tube," Ph.D. Thesis, Univ. of Queensland, Brisbane, Australia, 1995.

[32] McIntosh, M., "A Computer Program for the Numerical Calculation of Equilibrium and Perfect Gas Conditions in Shock Tunnels," Australian Defence Scientific Service, TR CPD 169, Canberra, Australia, 1968.

[33] Vardavas I. M., "Modeling Reactive Gas Flows Within Shock Tunnels," *Australian Journal of Physics*, Vol. 37, No. 2, 1984, pp. 157–177.

[34] Rizkalla, O., *EQSTATE: Program to Calculate the Equilibrium or Frozen Properties of a Supersonic Gas Flow at the Static and Stagnation Points Upstream and Downstream of a Shock Wave*, General Applied Science Labs., New York, 1990.

[35] Cohen, C. B., and Reshotko, E., "Similar Solutions for the Compressible Laminar Boundary Layer with Heat Transfer and Pressure Gradient," NACA TR-1293, 1956.

[36] Srivastava, A. C., and Hazarika, G. C., "Shooting Method for Third Order Simultaneous Ordinary Differential Equations with Application to Magneto-Hydrodynamic Boundary Layer," *Defence Science Journal*, Vol. 40, No. 3, 1990, pp. 263–274.

[37] Crocco, L., and Lees, L., "A Mixing Theory for the Interaction Between Dissipative Flows and Nearly Isentropic Streams," *Journal of the Aerospace Sciences*, Vol. 19, 1952, pp. 649–676.

[38] Holden, M. S., "Establishment Time of a Laminar Separated Flow," *AIAA Journal*, Vol. 9, No. 11, 1971, pp. 2296–2298. doi:10.2514/3.6512

[39] Lee, J. Y., and Lewis, M. J., "Numerical Study of the Flow Establishment Time in Hypersonic Shock Tunnels," *Journal of Spacecraft and Rockets*, Vol. 30, No. 2, 1993, pp. 152–163. doi:10.2514/3.11523

[40] Fuller, F. B., "Numerical Solutions for Supersonic Flow of an Ideal Gas Around Blunt Two-Dimensional Bodies," NASA TN D-791, July 1961.

[41] Belotserkovskii, O. M., "Flow Past a Circular Cylinder with a Detached Shock Wave," Research and Advanced Development Div., Avco Corp., Rept. RAD-9-TM-59-66, Wilmington, MA, Sept. 1959.

[42] Whitfield, J. D., and Potter, J. L., "on Base Pressure at High Reynolds

Numbers and Hypersonic Mach Numbers," Arnold Engineering Development Center, TN-60-61, Arnold Air Force Station, TN, March 1960.

[43] Koppenwallner, G., "Hypersonic Aerothermodynamics—Fundamentals of Hypersonics: Aerodynamics and Heat Transfer," *von Karman Institute for Fluid Dynamics Lecture Series 1984-01*, Rhode-Saint-Genèse, Belgium, Feb. 1984.

[44] White, F. M., *Viscous Fluid Flow*, New York: McGraw–Hill, New York, 1974.

[45] Truitt, R. W., *Fundamentals of Aerodynamic Heating*, Ronald Press, New York, 1960.

[46] Bashkin, V. A., Egorov, I. V., Egorova, M. V., and Ivanov, D. V., "Supersonic Laminar-Turbulent Gas Flow Past a Circular Cylinder," *Fluid Dynamics*, Vol. 35, No. 5, 2000, pp. 652–662. doi:10.1023/A:1026630613133

[47] Potter, J. L., "The Transitional Rarefied-Flow Regime," *Proceedings of the 5th International Symposium on Rarefied Gas Dynamics*, Sec. 3, Univ. of Oxford, Oxford, 1966.

[48] Wu, M. H., Wen, C. Y., Yen, R. H., Weng, M. C., and Wang, A. B., "Experimental and Numerical Study of the Separation Angle for Flow Around a Circular Cylinder at Low Reynolds Number," *Journal of Fluid Mechanics*, Vol. 515, 2004, pp. 233–260. doi:10.1017/S0022112004000436

[49] Batt, R. G., and Kubota, T., "Experimental Investigation of Laminar Near Wakes Behind 20° Wedges at $M_\infty = 6$," *AIAA Journal*, Vol. 6, No. 11, 1968, pp. 2077–2083. doi:10.2514/3.55432

[50] Zakkay, V., and Cresci, R. J., "An Experimental Investigation of the Near Wake of a Slender Cone at $M_\infty = 8$ and 12," *AIAA Journal*, Vol. 4, No. 4, 1966, pp. 41–46.

A. Tumin
Associate Editor